Geoscience Frontiers 5 (2014) 193–203

Contents lists available at SciVerse ScienceDirect

China University of Geosciences (Beijing)

Geoscience Frontiers

journal homepage: www.elsevier.com/locate/gsf

Research paper

Multitaper spectral method to estimate the elastic thickness of South China: Implications for intracontinental deformation

Yangfan Deng [a,b,*], Zhongjie Zhang [a], Weiming Fan [b], Marta Pérez-Gussinyé [c]

[a] State Key Laboratory of Lithospheric Evolution, Institute of Geology and Geophysics, Chinese Academy of Sciences, Beijing 100029, China
[b] Guangzhou Institute of Geochemistry, Chinese Academy of Science, Guangzhou 510640, China
[c] Department of Earth Sciences, Royal Holloway, University of London, Egham TW20 0EX, UK

ARTICLE INFO

Article history:
Received 30 November 2012
Received in revised form
16 May 2013
Accepted 21 May 2013
Available online 10 June 2013

Keywords:
South China
Effective elastic thickness
Spectrum estimation
Heat flow
Seismicity

ABSTRACT

The effective elastic thickness (Te) represents the thickness of the elastic layer or the flexural rigidity of the lithosphere, the equivalent of which can be calculated from the spectral analysis of gravity and topographic data. Studies of Te have profound influence on intracontinental deformation, and coupling of the tectonic blocks. In this paper, we use the multitaper spectral estimation method to calculate the coherence between Bouguer gravity and topography data, and to obtain the Te map of South China. Through the process of correction, we discuss the relationships of Te versus heat flow, and Te versus seismicity. The results show that Te distribution of South China is affected by three factors: the original age, which controls the basic feature; the Mesozoic evolution, which affects the Te distribution; and the neotectonic movement, which shaped the final distribution. The crust age has a positive correlation with the first-order Te distribution; thus the Yangtze Craton has a relatively higher Te (about 50 km) whereas the Te in Cathaysia block is only 10–20 km. By analysis and comparison among the tectonic models of South China, the Te distribution can be well explained using the flat-subduction model. As is typical with neotectonics, the region with a higher heat flow is related with a lower Te. The seismicity does not have a clear relationship with Te, but the strong seismicity could cause a low Te. Seismogenic layer (Ts) has a similar trend as Te in the craton, whereas in other areas the relationship is complex.

1. Introduction

Plate tectonics is based on the observation that the Earth's outermost layers, or lithosphere, can be divided into a number of plates (Watts and Burov, 2003). The effective elastic thickness (Te) of the lithosphere is the thickness of an ideal elastic plate that would bend by the applied loads for the long periods ($>10^5$ yr) of the geological time (Burov and Diament, 1995; Watts, 2001; Watts and Burov, 2003). It is the measurement of the resistance to deformation of the lithosphere, as well as flexure rigidity. Evaluation of Te is important as it has profound influence on intracontinental deformation and coupling of the different tectonic blocks. In the oceans, where the composition and thermal evolution of the lithosphere are relatively simple, the effective elastic thickness (Te) increases as the ages become older, and is approximately equal to the depth of the 450–600 °C oceanic isotherm based on the cooling plate model (McKenzie and Nimmo,1997; Watts and Burov, 2003). In contrast to the oceanic lithosphere, the continental lithosphere is relatively old and has a multilayer rheology feature, and its flexural rigidity does not depend on a single controlling parameter such as thermal age, but is an integrated effect of a number of other factors including the geotherm, crustal thickness, and composition (Burov and Diament, 1995; Watts and Burov, 2003; Pérez-Gussinyé et al., 2007, 2009a,b).

Earth structure is commonly imaged using seismic tomography, receiver function, and deep seismic or magnetotelluric sounding. The Te primarily depends on crustal compositions and parameters of power law creep. Thus, Te could be used, in principle to map

* Corresponding author. State Key Laboratory of Lithospheric Evolution, Institute of Geology and Geophysics, Chinese Academy of Sciences, Beijing 100029, China. Tel.: +86 (0) 10 82998345.
E-mail addresses: dengyangfan@mail.iggcas.ac.cn, yangfandeng345@gmail.com (Y. Deng).

Peer-review under responsibility of China University of Geosciences (Beijing)

Production and hosting by Elsevier

1674-9871/$ – see front matter © 2013, China University of Geosciences (Beijing) and Peking University. Production and hosting by Elsevier B.V. All rights reserved.
http://dx.doi.org/10.1016/j.gsf.2013.05.002

lithospheric structure in an analogous way as seismic velocities and conductivities. As Te represents a depth integral of rheological strength over the lithosphere, it offers a unique view of the lithospheric structure. Recently, mapping lithospheric flexural rigidity at continent-wide scale has become more convenient because of the availability of relatively high resolution, low noise satellite-derived global gravity data that can be combined with terrestrial data (Pérez-Gussinyé et al., 2007).

The Te studies of South China are in the beginning stage. Mao et al. (2012) initiated the first study using wavelet method. However, the results were not adequate to understand the complex intracontinental deformation in the continental lithosphere under long-term tectonic processes. In this paper we map the Te distribution using multitaper spectral estimation method, and compare the results with seismogenic layer (Ts). Furthermore, we investigate the relationship of Te versus terrane age and other proxies for lithospheric structure such as heat flow. Finally, we discuss the spatial correlation between Te and intracontinental seismicity, and its significance for geotectonic deformation of the continental interior.

2. Geological setting

South China is located in the southeast of Eurasian continent with the Tibetan Plateau to the west (Fig. 1). It is an important part of the tectonic framework in the continental margin of eastern Asia and carries three Triassic–Jurassic orogens: the Qinling–Dabie orogenic belt along its northern margin, which records the collision with North China; the Longmenshan belt along its northwestern margin, possible related to the crust flow of the Tibetan Plateau; and the South China fold belt, where the tectonic units have a broad northeastward trend (Li, 1994a,b; Li and Li, 2007; Zhang et al., 2009, 2011, 2012; Li et al., 2012a,b; Wang et al., 2013). South China was formed by collision between the Yangtze and Cathaysia blocks at around 0.8–1 Ga (Zhou and Zhu, 1993; Li et al., 2002). Several Mesozoic granitoids and volcanic rocks occur in the region, and the outcrop area of the Triassic granitoids is about 15,000 km^2, accounting for ~7% of the total exposed Mesozoic granitoids in South China (Wang et al., 2003; Mao et al., 2012). The Yangtze Craton collided along its northern margin with the Sino-Korean platform during the early Triassic (Kenneth and Chen, 1999; Kim et al., 2011).

Since multiple phases of deformation (Wang, 2009; Li et al., 2012a,b), metamorphism (Shen et al., 1993) and magmatism (Li and Li, 2007; Wang and Shu, 2012) occurred in the crustal-scale process, South China is one of the ideal regions to study continental reworking (Cawood et al., 2009). The final tectonic frame of South China was influenced by the west Pacific Plate subduction, and controlled by the collision between Indian and Eurasia plates (Northrup et al., 1995; Wang, 2009; Deng et al., 2011). Previous studies show that the early deformation in South China was mainly NE (from Permian to Jurassic), which switched to NW later during the Triassic to Cretaceous (Wang, 2009; Deng et al., 2011).

3. Methodology and data

The lithosphere is composed of several coupled or uncoupled layers, and every layer has its flexural rigidity. Therefore, the Te reflects an integral of elastic strength at each lithospheric layer, which is constrained by the brittle and ductile rheology of the lithosphere (Burov and Diament, 1995; Lowry and Smith, 1995).

Te of the lithosphere is a convenient measure of the flexural rigidity (D), which is the resistance to bending under applied loads. The two are related by the equation

$$D = \frac{E\mathrm{Te}^3}{12(1-\sigma^2)} \quad (1)$$

where the elastic constants E and σ are Young's modulus and Poisson's ratio, respectively.

There are two main approaches in the estimation of Te: the direct and spectral approaches (Audet and Mareschal, 2007). The former involves computing the gravity anomalies of the

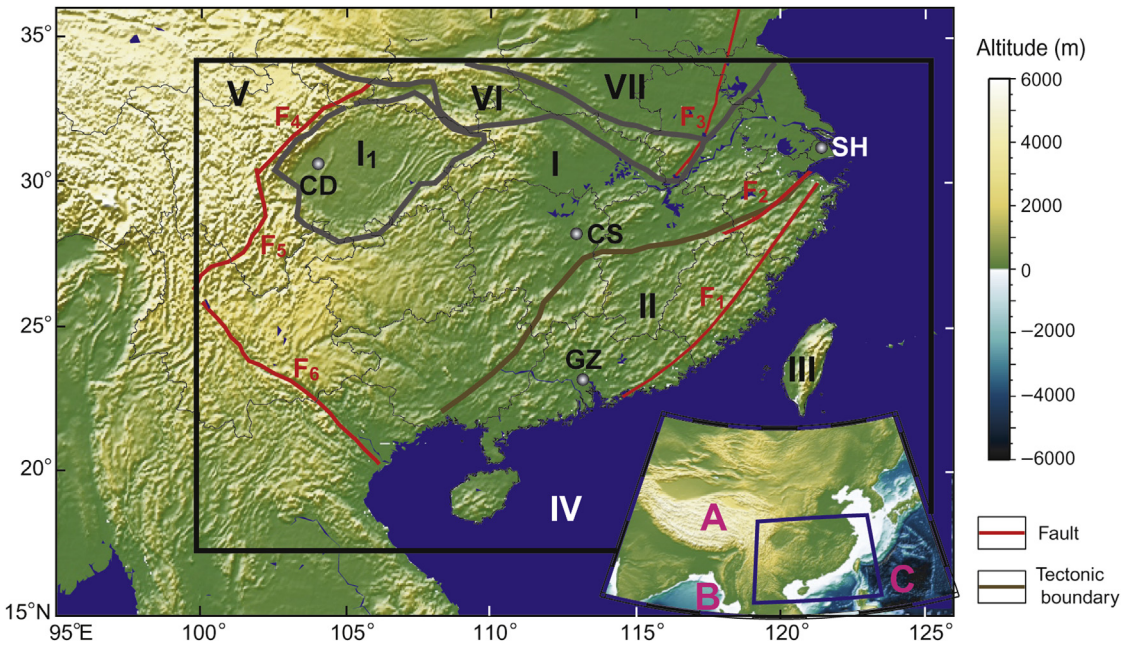

Figure 1. The geological background of South China and adjacent region. The area studied this paper is outlined with black rectangle. A: Asian plate; B: Indian plate; C: Philippine sea plate; I: Yangtze block; II: Cathaysia block; III: Taiwan orogen; IV: South China Sea basin; V: East of Songpan-Ganzi fold; VI: Qinling–Dabie orogen; VII: North China block; I_1: Sichuan Basin; F_1: Zhenghe-Dapu fault belt; F_2: Jiangshan-Shaoxing fault belt; F_3: Tanlu fault belt; F_4: Longmenshan fault belt; F_5: An'ninghe fault belt; F_6: Honghe fault belt; CD: Chengdu city; CS: Changsha city; SH: Shanghai city; GZ: Guangzhou city.

assumed tectonic loading and comparing with the observed gravity field to infer the mechanical properties of the lithosphere. This method is useful for certain geological settings such as mountain belts, seamounts and sedimentary basins, where the loading structure is well known (Jin et al., 1996; Watts and Burov, 2003; Jiang and Jin, 2005; Jordan and Watts, 2005). The other is calculating the spectrum between topography and gravity anomaly. Following Forsyth (1985), the majority of researchers use the coherence between Bouguer gravity and topography to estimate Te, because it allows the decomposition of the loads into surface and internal components and is less sensitive to short wavelength noise in the coherence between Bouguer gravity and topography than the admittance between free-air gravity and topography. The coherence between two fields is defined in the Fourier transform domain as

$$\gamma^2_{\mathrm{obs}} = \left\langle \frac{S_{\mathrm{hb}}(k)^2}{S_{\mathrm{hh}}(k)S_{\mathrm{bb}}(k)} \right\rangle \quad (2)$$

where $S_{\mathrm{hb}}(k)$, $S_{\mathrm{hh}}(k)$, $S_{\mathrm{bb}}(k)$ are the cross-power spectrum of the topography, Bouguer anomaly and the auto-power spectra of the topography, the Bouguer anomaly, respectively. Angle brackets denote averaging over annular wave number modulus

$$k = |k| = \sqrt{k_x^2 + k_y^2}$$

For uncorrelated regions, the phases of the cross-spectra at a given wave number are randomly distributed and averaging decreases the coherence. For correlated regions, the phases of the cross-spectra interfere constructively and averaging yields a high coherence. At short wavelengths, where topographic and internal mass anomalies are uncompensated, the coherence generally tends to zero. At long wavelengths the response to loading approaches the Airy limit and the coherence tends to one (Forsyth, 1985). The wavelengths at which coherence increases from 0 to 1 depend on load distribution and the effective elastic thickness, Te, of the lithosphere. As shown in Fig. 2a, the topography is uncorrelated with Bouguer gravity, so the coherence is zero, and the Te tends to ∞; from Fig. 2b, the topography is wholly correlated with Bouguer gravity, which corresponds to Airy compensation, the coherence is one, and Te is zero; Fig. 2c reflects the actual problems, and at these cases $0 <$ coherence < 1, $0 <$ Te $< \infty$.

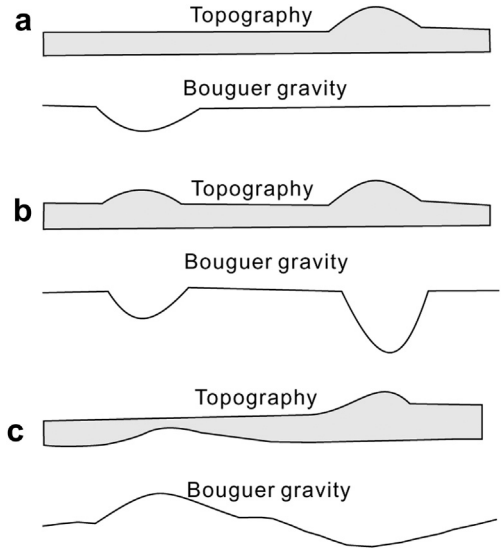

Figure 2. Sketch of flexural model. (a) The topography is uncorrelated with Bouguer gravity, so the coherence is zero, and the Te tends to ∞; (b) the topography is wholly correlated with Bouguer gravity, which corresponds to Airy compensation, the coherence is one, and Te is zero; (c) reflects the actual problems, and at these cases $0 <$ coherence < 1, $0 <$ Te $< \infty$.

The spectral method is composed of two steps. First, assigning the Te that minimizes the difference between the predicted and observed coherence for an analyzed area. To calculate the predicted coherence, assumptions about the loading processes in the lithosphere need to be made. Wherein, surface loads (atop the lithosphere) and subsurface loads (within the lithosphere) are considered statistically uncorrelated (Forsyth, 1985). Surface loads include the thrust sheets that comprise topography in orogenic belts, while subsurface loads occur in a wide range of geological settings (Watts, 2001). In compressional settings, they include the overthrusting of large crustal blocks that causes large-scale flexing of the lithosphere. In extensional settings, they include the effects of heating the lithosphere as magmatic underplating. For any given Te, we calculate a set of surface and subsurface loads and compensating deflections that reproduce exactly the observed topography and gravity anomaly, an approach commonly known as load deconvolution (Forsyth, 1985). Forsyth's (1985) original formulation of the predicted coherence assumes that all internal density variation and loading occur at the Moho. So we used CRUST2.0 (Bassin, 2000) to define the internal density profile and assumed that internal loading occurs at the interface between upper and mid-crust. The lateral variation in depth of this interface was obtained from CRUST2.0. Since the observed coherence can be reproduced equally well by either low Te and shallow loading or a larger Te and deeper loading, there is a trade-off between Te and assumed depth of loading. However, Pérez-Gussinyé and Watts (2005) have tested the sensitivity of Te to loading depth in Europe and found that changing the loading depth from the mid-crust to Moho changed Te by ~5 km, but the general patterns of variations remained the same.

In addition, the coherence function is a normalized cross-power spectrum of the Bouguer gravity and the topography. Hence it involves transformation of the two data sets into the Fourier domain to estimate their auto- and cross-power spectra. Because both data sets are nonperiodic and finite, the Fourier transformation of this windowed data introduces leakage, or transference of power between neighboring frequencies, resulting in estimated spectra that differ from the true spectra. To reduce leakage, the data are first

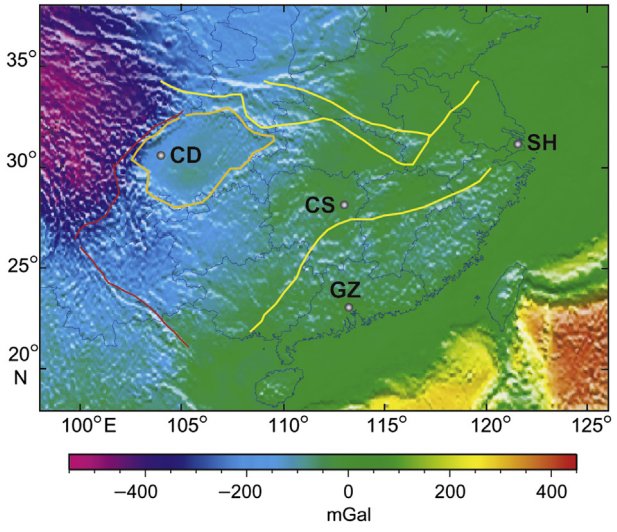

Figure 3. The Bouguer gravity of South China and adjacent region. The tectonic units are the same as Fig. 1. CD: Chengdu city; CS: Changsha city; SH: Shanghai city; GZ: Guangzhou city.

multiplied by a set of orthogonal tapers in the space domain, the Fourier transform of the data-taper product taken for each taper, and the power spectrum determined at each taper. The final estimate of the signal's true power spectrum is then the weighted average of the individual power spectra over all tapers. However, ultimately, the type of taper used influences slightly the resulting power spectra and hence the coherence functions. In this paper we use a multitaper scheme corresponding to NW = 3, which is also used in many other studies for Te estimation (Audet and Mareschal, 2004; Pérez-Gussinyé et al., 2004, 2008; Pérez-Gussinyé and Watts, 2005).

The previous works confirm that the multitaper method can recover more accurate Te than the periodogram method or simple Hanning taper (Pérez-Gussinyé et al., 2004), and has similar lateral resolution to the high-resolution wavelet method with steep Te gradients and small scale Te anomalies (Pérez-Gussinyé et al., 2009a; Kirby and Swain, 2011).

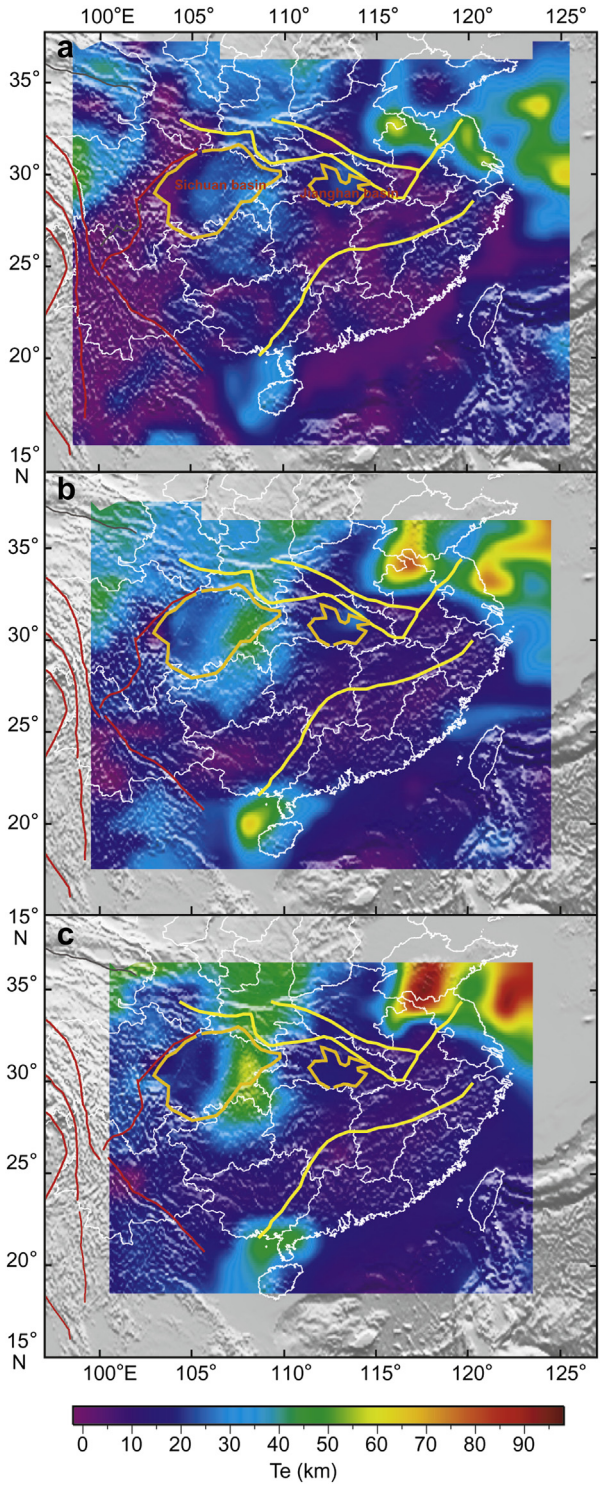

Figure 4. Te estimates in South China using (a) 400 km × 400 km windows; (b) 600 km × 600 km windows; (c) 800 km × 800 km windows. The tectonic units are the same as Fig. 1.

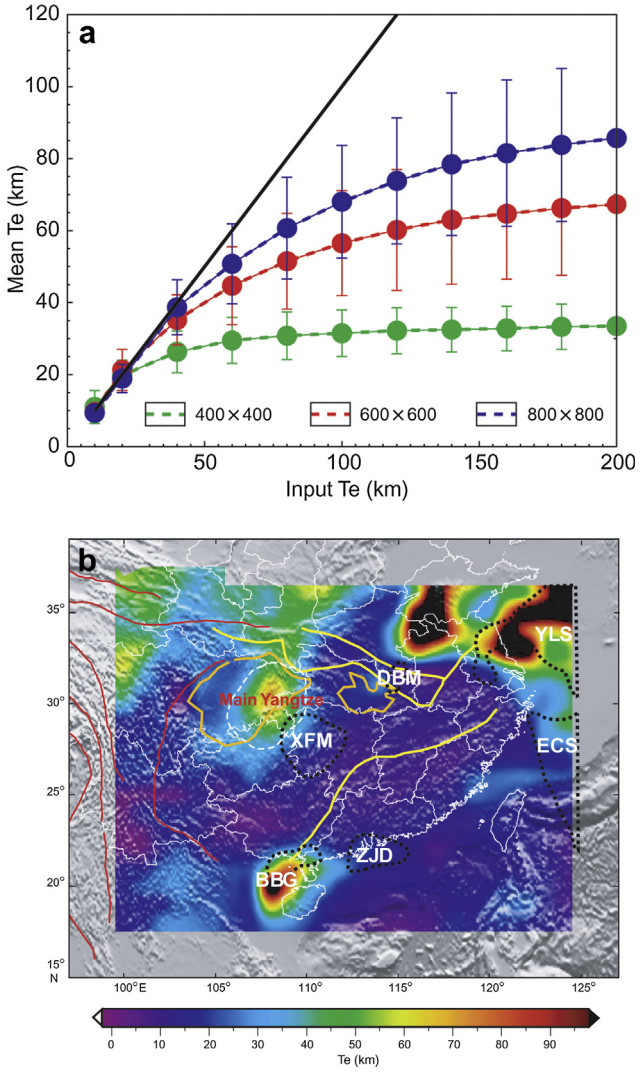

Figure 5. (a) Mean Te estimate and standard deviation versus input Te, from tests with 100 synthetic topography and Bouguer anomaly data sets generated using spatially constant input Te values of 10, 20, 40, 60, 80, 100, 120, 140, 160, and 200 km. Green, red, and blue indicate the results of the calculation using windows sizes of 400 km × 400 km, 600 km × 600 km, and 800 km × 800 km, respectively. The black line shows perfect recovery. The standard deviations increase with input Te, as the coherence transition wavelength for those Te values increases relative to the window aperture used for analysis. We fit a regression curve to the mean Te values to define a correction for the downward bias resulting from the limited window size. (b) Te distribution after correction from 600 km × 600 km windowed estimates. The tectonic units are the same as Fig. 1. The white dotted line outlines the high Te region as main Yangtze; the dashed black areas have the maximum of normalized squared imaginary part of the coherency between free-air gravity anomaly and topography, and in which possible influence of significant noise would be on the Te results (Mao et al., 2012). XFM: Xuefeng Mountain; DBM: Dabie Mountain; YLS: Yellow Sea; ECS: East China Sea; BBG: Beibu gulf basin; ZJD: Zhujiang delta.

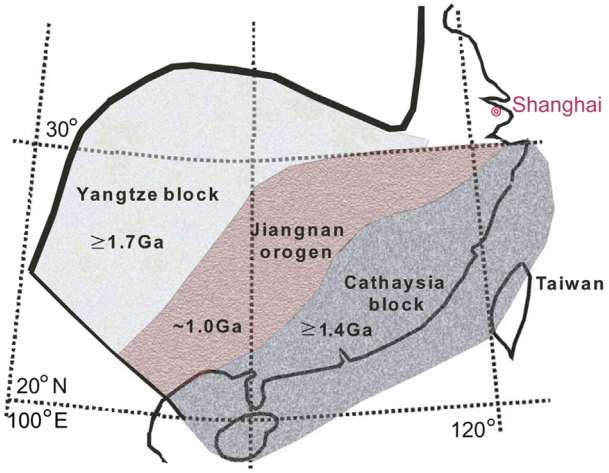

Figure 6. The first-order crust age of South China.

The topography data (Fig. 1) are from Etopo1 (www.ngdc.noaa.goc/mgg/global/global.html) with resolution 1′ × 1′. The Bouguer gravity data (Fig. 3) are from EGM2008 (Pavlis et al., 2008), which provides 2.5′ × 2.5′ grid on both land and ocean, including synthetic gravity generated by GRACE and terrestrial gravity anomaly; the standard deviations of the data are smaller than 5 mGal. In South China, small positive gravity anomalies (<100 mGal) are confined to regions near the ocean and the sea area. At a larger scale, small negative gravity anomalies (about −200 mGal) can be observed in part of the Qinling–Dabie orogen, Sichuan basin; already in the Songpan-Ganzi block, the Bouguer gravity shows progressively more negative values westwardly, up to reach −550 mGal. Thus, it can be summarized that the elevation is higher, the gravity anomaly is lower.

4. Results and correction

From a series of synthetic tests, we find that if Te is uniform everywhere, and that the result with large windows would yield

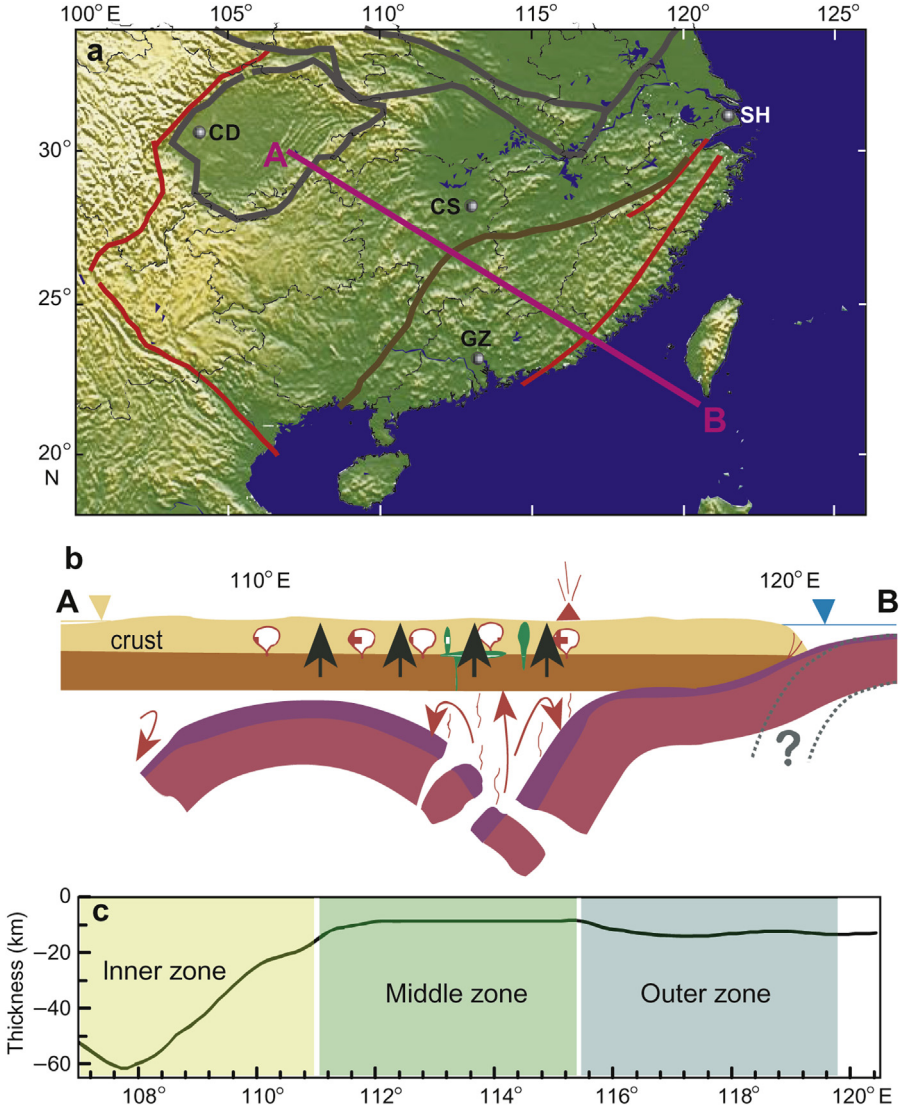

Figure 7. The elastic thickness versus the flat-subduction model, (a) the position of the transect, (b) the flat-subduction model along transect AB, (c) the elastic thickness along transect AB, inner zone, middle zone and outer zone are distinguished according to the distance to A point. The tectonic units are the same as Fig. 1. CD: Chengdu city; CS: Changsha city; SH: Shanghai city; GZ: Guangzhou city.

more accurate estimates. However, Te certainly varies at different places. Since Te is assumed as a constant within the data windows used for estimation, we can obtain a weighted average of the spatially varying Te from estimations of different places (Pérez-Gussinyé et al., 2004, 2009a,b). Hence the choices of different window size decided the trade-off between resolution and variance of the estimation results. A larger window is better to retrieve high Te, and a smaller window is better to retrieve the spatial variations. However, because the variance of the spectra increases with decreasing data window size, a smaller window may yield spurious spatial variations (Pérez-Gussinyé et al., 2004, 2009a,b). While the larger window smoothes the estimate and probably attenuates real structure (Pérez-Gussinyé et al., 2004, 2008). To evaluate the effects of different window sizes, we estimate Te with three different window sizes and interpret only those Te variations that persist in the results with all the three windows as shown in Fig. 4a–c.

Although the first-order pattern of spatial variance in Te remains similar for the results using three different estimation windows, there are differences in the small extent of the imaged structures as well as the mean Te recovered, in analogous to the synthetic data recovered (Pérez-Gussinyé et al., 2004). The smallest window yields a highly variable Te pattern within the continental interior. Besides, at the same high Te area, the larger window will lead to a higher Te. However, all three windows have low Te in the Cathaysia block, and high Te in the Sichuan and Jianghan basin. Specifically, the Te result in the estimation of 400 km × 400 km window ranges from 5 km to 50 km, accompanied with spurious spatial variance. And the result in the 600 km × 600 km windowed estimate is in between 5 km and 70 km; 5–90 km distributes in the 800 km × 800 km windowed estimate, where the data are too smoothed to identify the local geological structure.

Previous studies where the mean Te and the standard deviation from simulations with 100 synthetic topography and Bouguer anomaly data sets were generated using spatially constant input Te of 10, 20, 40, 60, 80, 100, 120, 140, 160 and 200 km, show that as the input Te increases for a given analysis window, both the downward bias error and the estimate uncertainty increase (Fig. 5a). To remove the bias related to windowing, we fit a regression curve to the mean Te values to define a correction for the downward bias resulting from the limited window size. Pérez-Gussinyé et al. (2009a) gave detailed information about this correction method, which could be briefly descried as adding the difference between the input Te and the recovered Te performed into the synthetic experiments. The incidence of outliers due to Fourier transform edge effects is found to be much greater in synthetic data than in real data (Pérez-Gussinyé et al., 2009a). Now, we make this correction on the 600 km × 600 km windowed estimation, and get Fig. 5b as the final result for the following discussion.

As pointed out by Kirby and Swain (2009), significant noise generally appears in subdued regions. Such noise is found in the regions with low topography variance, such as the Yellow Sea, the East China Sea, the Beibu gulf basin and the Zhujiang delta region near the south coastline of South China. Furthermore, Mao et al. (2012) calculated maximum of normalized squared imaginary part of the coherency between free-air gravity anomaly and topography for three wavelengths and suggested that significant noise also exists in regions with sharp topography, e.g., in the Dabie Mountain, the Xuefeng Mountain (western part of the Jiangnan Neoproterozoic orogenic belt), and the Ryukyu Trench, which are all convergent boundaries. Consequently, other estimate of the corrected Te is reliable.

The Yangtze Craton is an old and strong cratonic block, and plays an important role in preventing the eastward flow of Tibet (Zhang et al., 2009). Only a part of Yangtze Craton shows high Te value (marked with white dotted line in Fig. 5b). We term this region as the main Yangtze, and suggest that this region maintained its rigidity since Mesozoic, whereas the other areas underwent disruption or erosion resulting in their rigidities becoming weaker.

5. Discussion

5.1. Te and tectonic province

South China is believed to have formed through the collision between the Yangtze and Cathaysia blocks. A number of possible ages for the collision have been proposed, among which the ca. 1000 Ma and 800 Ma range are most widely accepted (Li et al., 1995, 2002), coinciding with time of global Grenville orogeny. From the geochemical and geochronologic data, the Yangtze block is confirmed to have a late Archean–Paleoproterozoic (≥1.7 Ga) nucleus surrounded by younger orogenic belts (Li et al., 1995). Isotopic studies in the past decade indicate the existence of a pre-1.4 Ga continental crust (John et al., 1990; Li, 1994a), although the nature and age of the Cathaysia block are more complicated, and it is possible to map out the first-order age of South China, as shown in Fig. 6.

The Yangtze block has the highest Te value varying 10–50 km, whereas the Cathaysia block has the Te about 5–20 km, and the collision orogen (Jiangnan orogen) between them has the lowest Te, 5–10 km. In summary, the Te is higher in which the continent is older.

5.2. Te and Mesozoic evolution

Because the intracontinental lithosphere and flexural rigidity will be deformed, even destructed by the tectonic process, the reasonable model should explain the Te distribution well. Several models have been postulated to account for the Mesozoic tectonic evolution of South China. These models include Andean-type continental margin (Guo et al., 1983), Alps-type collision belt (Hsü et al., 1988, 1990) and lithospheric subduction (Holloway, 1982; Zhou and Li, 2000). Recently Li and Li (2007) proposed a flat–slab subduction model for Mesozoic South China based on new sensitive high-resolution ion microprobe (SHRIMP) U–Pb zircon data and a synthesis of existing structural geochronological, and sedimentary facies studies. The model can explain not only the

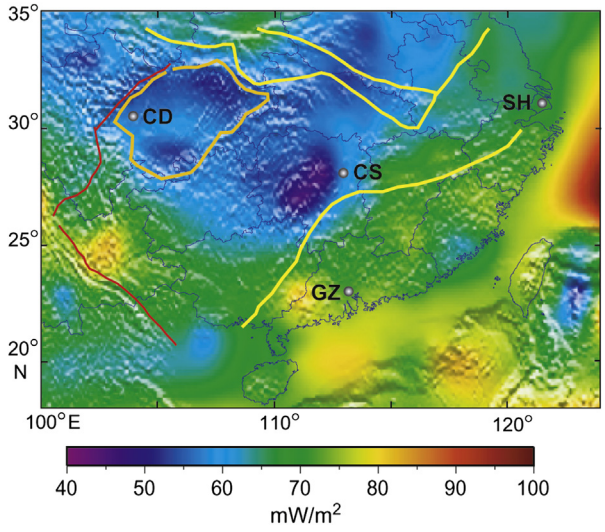

Figure 8. The heat flow of South China. The tectonic units are the same as Fig. 1. CD: Chengdu city; CS: Changsha city; SH: Shanghai city; GZ: Guangzhou city.

broad (1300 km) intracontinental orogen that migrated from the coastal region into the continental interior, but also the development of one of the world's largest Basin and Range-style magmatic provinces after the orogeny (Wang and Shu, 2012). Li et al. (2012a,b) suggested that the normal subduction along the continental margin was resumed after the flat–slab subduction based on new age data from granite bodies in coastal South China and Taiwan, as well as the sedimentary provinces.

The model and its corresponding location are shown in Fig. 7. We divided the profile into three parts according to the distance to point A, as inner zone, middle zone and outer zone (Fig. 7c). The thickness of Te shows a remarkable relationship with the model. As an active plate, the Pacific plate subducts along the coastline under the South China (Li and Li, 2007), so the outer zone also can be named as contact zone. The deformation of the outer zone is not remarkable because of the flat-subduction, and the Te in this zone is about 10–15 km. The middle zone is the most affected region of the model, because large-scale anorogenic magmatism (including alkaline basalts, bimodal volcanic rocks, and I- and A-type granites) was evolved through to the full-scale slab foundering (Li and Li, 2007). Thus, the lithosphere suffered extensive destruction, and the rigidity of rocks will be weaker, reflected in the low Te value in this area (<10 km). The extent of this destruction was not transmitted into the inner zone from southeast, and there is no obvious magmatic destruction, so the composition and flexural rigidity were preserved. Thus, the Te is highest in this region, with the value up to 60 km.

5.3. Te and surface heat flow

Heat flow is the heat transferred in a unit time from the earth interior to the surface, which is equal to the temperature multiplied by thermal conductivity, and its unit is mW/m^2. It is also the most direct display of the internal heat process in the earth, carrying

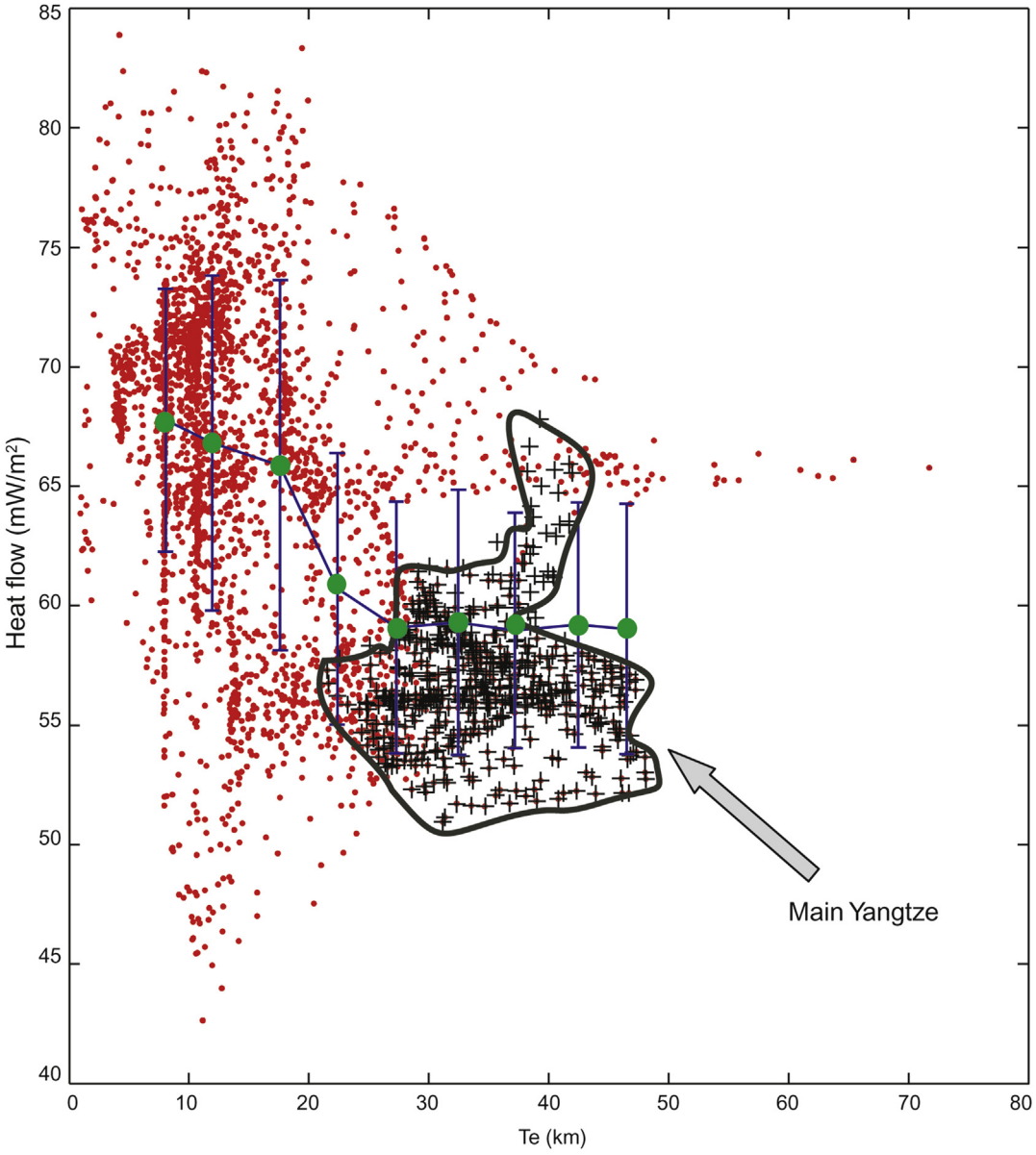

Figure 9. Red dots are scatter plots of Te estimates obtained using 600 km × 600 km windows versus heat flow in South China. Green circlers represent the mean Te within 5 km interval versus mean heat flow; bars indicate the standard deviation. In all, the mean heat flow is inversed to the mean Te. The black crosses outline the Te and heat flow value in the main Yangtze.

important geological, geophysical and geodynamic information (Lowry and Smith, 1995). In general, stronger tectonic activity in a region would lead to higher heat flow. The heat flow values in stable cratons are low (Wang, 2001). The distribution of heat flow is of great significance to understand the crust temperature gradient and mantle convection. However, uncertainties about the relationship between surface heat flow and temperature at depth can be large, because of poorly known crustal heat production, dynamical effects of subduction, erosion, and hydrologic flow (Mareschal and Jaupart, 2004). Wang (2001) summarized the heat flow data for the whole of China, and Tao and Shen (2008) presented the heat flow map in China mainland with resolution of 1° × 1° based on previous works. Here we present the heat flow map (Fig. 8) using the data from Tao and Shen (2008).

Compared with the Te distribution in Fig. 5b, the negative correlation between heat flow and Te is remarkable. For example, low heat flows occur in the Upper Yangtze, corresponding to the high Te, and the high heat flows in Cathaysia block match the low Te (Fig. 8). Consequently, we infer a correlation between heat flow and Te in Fig. 9, where the green circlers represent the mean Te within 5 km interval versus. The mean heat flow is inversed to the mean Te. The main Yangtze domain is located in the region that displays high Te and low heat flow.

5.4. Te and seismicity

If the lithosphere behaves as an elastic plate, then the plate structure may be reflected in seismicity data, because seismicity is the consequence of frictional instabilities in sliding surfaces such as faults. The bending stress induced by flexural loading might be one possible source for the reason that could cause faulting (Watts, 2001). On the other hand, the occurrence of earthquakes depends on the bending stress and the corresponding capacity. Thus, a positive correlation might exist between the Te and the depth interval over which earthquakes occur. However, strong seismicity could be the hint of a weaker plate because of the high brittleness.

The distribution of the earthquakes between 1980 and 2010 (data from China Earthquake Networks Center) is shown in Fig. 10a, and the numbers in each 1° × 1° grid are shown in Fig. 10b. The energy release by earthquakes is calculated using $E = \mathrm{ML} \times 1.5 + 11.8$ (Richter, 1958; Panza and Raykova, 2008), shown in Fig. 10c. A comparison of the seismicity with the Te results displays a complex relationship. The strong seismicity in the Longmenshan and Chuandian area corresponds to a relatively low Te value. However, the seismicity in the central part of South China is weak, and the Te is also low; the stable platform in the Sichuan basin has a high Te. We therefore infer that a strong seismicity probably leads to a low Te, and lack of seismicity does not necessarily imply that the lithosphere is more rigid. The relationship between seismicity and Te is complicated, and other factors must also be taken into account.

5.5. Te and seismogenic layer (Ts)

The depth at which 80% of earthquake energy is released is termed as Ts (Panza et al., 2003; Zhang et al., 2011, 2012, 2013; Deng et al., 2012; Wu and Zhang, 2012), which reflects the extent of faulting in the uppermost part of the lithosphere. Maggi et al. (2000) suggested that most of the earthquakes occur in the upmost crust, so Ts is likely to be limited to the uppermost 10–15 km of the crust. Ts may be deeper, depending on the level of the bending and/or in-plane tectonic stress (Watts and Burov, 2003). In contrast to Ts, Te reflects the integrated strength of the entire lithosphere, which includes a significant contribution from the aseismic part of the lithosphere, and the time scale exceeds

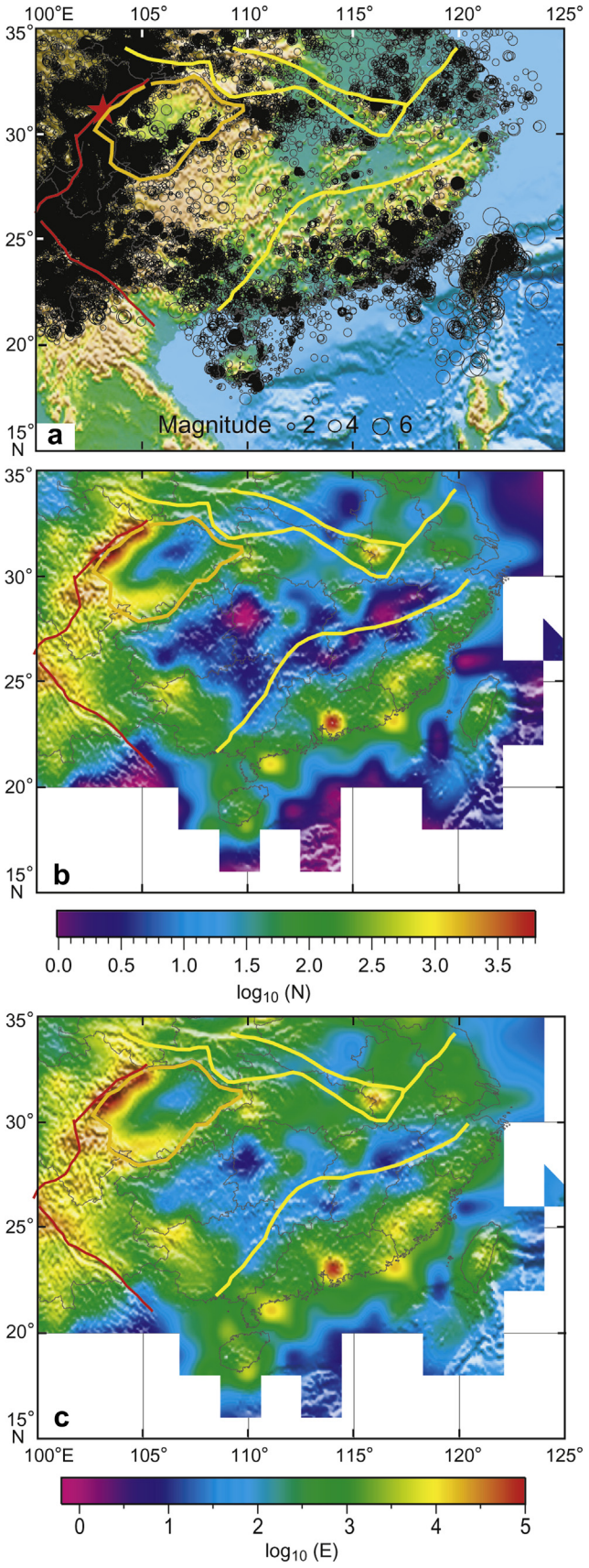

Figure 10. The seismicity of South China, (a) the distribution of earthquakes (1980–2010) in South China, (b) the earthquake number variation in South China by 1° × 1° grid, (c) the energy distribution in South China by 1° × 1° grid. The red star represents the position of 8.0 Ms earthquake at 2008.05.12. The tectonic units are the same as Fig. 1.

~10^5 yr. Generally, the strength of the lithosphere is determined by the extent of the brittle deformation and therefore that Ts is the same as Te (Maggi et al., 2000). Watts and Burov (2003) concluded that Te ≫ Ts in cratons, many convergent zones, and some rifts. Most rifts, however, are characterized by a low Te that has been variously attributed to a young thermal age of the rifted lithosphere.

Here we take a transect from Heishui to Quanzhou, which is an important part of Global Geological Transect (GGT), investigated with deep seismic sounding, gravity and other geophysical and geological survey (Cui et al., 1996; Deng et al., 2011). Fig. 11 shows the integral features of the Heishui–Quanzhou transect. The Moho depth gradually decreases eastward from 42 to 30 km, and the elevation undulates slightly, revealing the configuration of

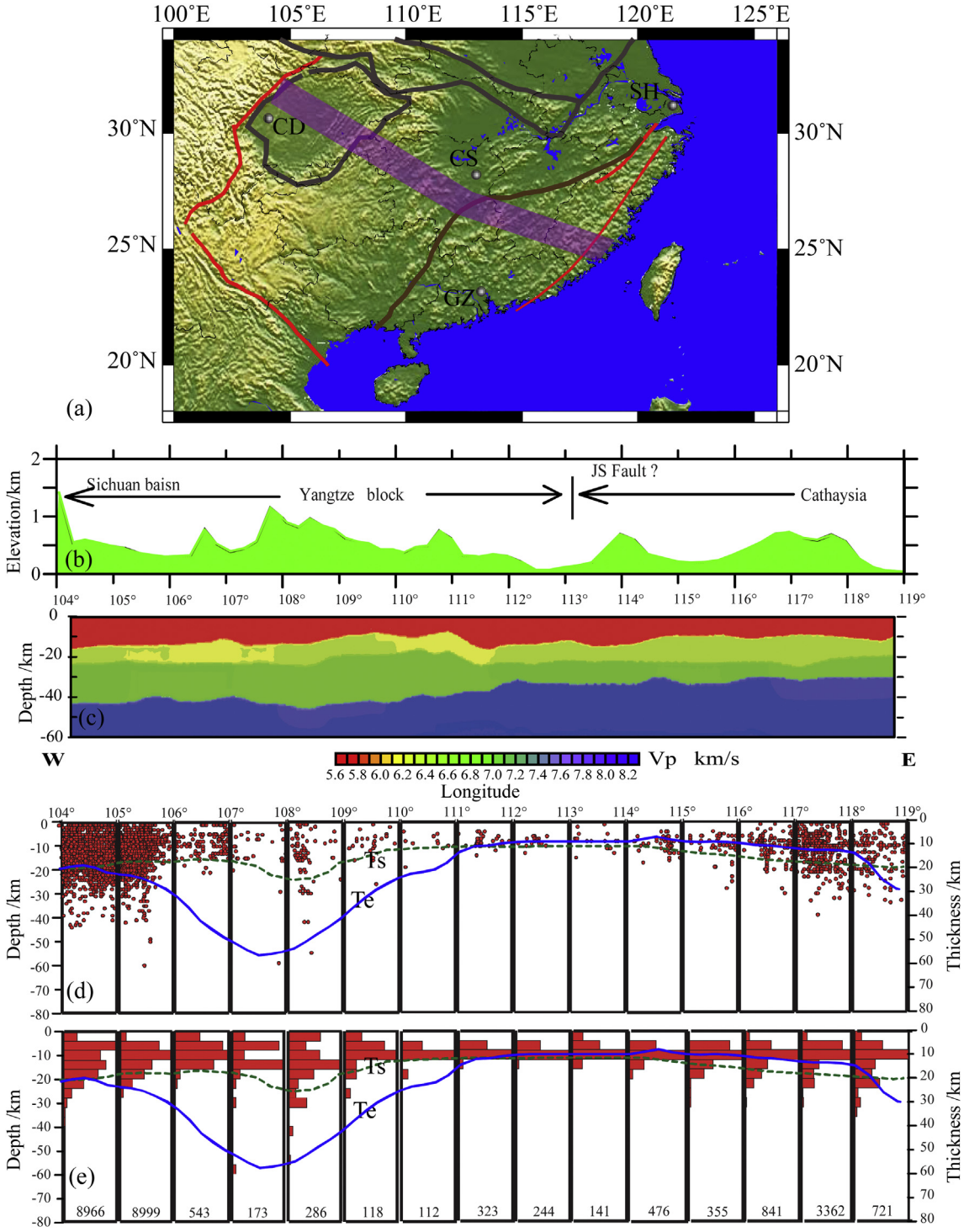

Figure 11. The geophysical features along the Heishui–Quanzhou transect. (a) The position of the transect, (b) the elevation, (c) the *P*-wave velocity, (d) the earthquake distribution versus depth, (e) the earthquake energy versus depth by 4 km interval. The numbers in each cell show the value of the maximum of each histogram when the earthquakes are sorted in 4 km depth intervals. The tectonic units are the same as Fig. 1. JS fault: Jiangshan-Shaoxing fault; CD: Chengdu city; CS: Changsha city; SH: Shanghai city; GZ: Guangzhou city.

intracontinental orogeny. It is seen that although the values of Ts and Te are not equal (the deepest Ts is 25 km, and the most thickness Te is about 50 km), the trend is consistent, where the Ts are deep, and the Te are thick. For the area with Ts > Te, the evolution may be related to magmatism since Mesozoic (Wang et al., 2003) where the heat flow is also relatively higher (Fig. 8).

6. Conclusions

We have estimated the Te structure of South China by modeling the coherence of topography and gravity anomaly with different windows, and discussed the relationship of Te versus heat flow and other proxy features.

Te distribution in South China is the comprehensive reflection of three elements, the original crust age (which controls the principal Te distribution), the Mesozoic evolution (which affects the Te distribution), and the neotectonic movement (which shaped the final Te distribution). The first-order Te distribution is consistent with the age of crust, with an older crust corresponding to a higher Te. The later geological and tectonic process exert key influence on the lithospheric rigidity. Thus, the old and rigid Yangtze Craton does not display a high Te. The Te value can be explained well with the flat-subduction model. The Te value is low in the magmatic destruction zone, and high in the stable zone. The heat flow and seismicity modify the Te distribution remarkably, for example a region with higher heat flow has lower Te, and a stronger seismicity could cause a lower Te. Though the trend of Te and Ts distributions are consistent in South China, the relationship between them is complicated.

Acknowledgments

We appreciate the great help in the interpretation of geodynamic processes made by Xiaofeng Liang, Lin Chen, and Jing Wu in IGGCAS and Alberto in the Universidad Complutense de Madrid. We are also thankful to Professor M. Santosh and two anonymous reviewers for their constructive suggestions and comments to improve the study and its presentation. The study was supported financially by the Ministry of Science and Technology of China (Sinoprobe-03-02) and the National Natural Science Foundation of China (Grant No. 41021063).

References

Audet, P., Mareschal, J.C., 2004. Variations in elastic thickness in the Canadian Shield. Earth and Planetary Science Letters 226 (1–2), 17–31.

Audet, P., Mareschal, J.C., 2007. Wavelet analysis of the coherence between Bouguer gravity and topography: application to the elastic thickness anisotropy in the Canadian Shield. Geophysical Journal International 168 (1), 287–298.

Bassin, C., 2000. The current limits of resolution for surface wave tomography in North America. Eos, Transactions American Geophysical Union 81, F897.

Burov, E.B., Diament, M., 1995. The effective elastic thickness (Te) of continental lithosphere: what does it really mean? Journal of Geophysical Research 100 (B3), 3905–3927. http://dx.doi.org/10.1029/94JB02770.

Cui, Z.Z., Chen, J.P., Wu, L., 1996. Memoirs of the Geoscience Transection for the Continental Lithosphere Beneath Altay–Taiwan. Geological Press, Beijing.

Cawood, P.A., Kröner, A., Collins, W.J., Kusky, T.M., Mooney, W.D., Windley, B.F., 2009. Accretionary orogens through Earth history. Geological Society, London, Special Publications 318 (1), 1–36.

Deng, Y.F., Li, S.L., Fan, W.M., Liu, J., 2011. Crustal structure beneath South China revealed by deep seismic soundings and its dynamics implications. Chinese Journal of Geophysics 54 (10), 2560–2574 (in Chinese with English abstract).

Deng, Y., Fan, W., Zhang, Z., Badal, J., 2012. Geophysical evidence on segmentation of the Tancheng-Lujiang fault and its implications on the lithosphere evolution in East China. Journal of Asian Earth Sciences. http://dx.doi.org/10.1016/j.jseaes.2012.11.1006.

Forsyth, D.W., 1985. Subsurface loading and estimates of the flexural rigidity of continental lithosphere. Journal of Geophysical Research 90 (B14), 12623–12632.

Guo, L., Shi, Y., Ma, R., 1983. On the formation and evolution of the Mesozoic–Cenozoic active continental margin and island arc tectonics of the western Pacific Ocean. Acta Geologica Sinica 57 (11) (in Chinese with English abstract).

Holloway, N., 1982. North Palawan block, Philippines – its relation to Asian mainland and role in evolution of South China Sea. American Association of Petroleum Geologists Bulletin 66 (9), 1355–1383.

Hsü, K.J., Shu, S., Jiliang, L., Haihong, C., Haipo, P., Sengor, A., 1988. Mesozoic overthrust tectonics in south China. Geology 16 (5), 418–421.

Hsü, K.J., Li, J., Chen, H., Wang, Q., Sun, S., Sengör, A., 1990. Tectonics of South China: key to understanding West Pacific geology. Tectonophysics 183 (1–4), 9–39.

Jiang, X., Jin, Y., 2005. Mapping the deep lithospheric structure beneath the eastern margin of the Tibetan Plateau from gravity anomalies. Journal of Geophysical Research 110 (B7), B07407.

Jin, Y., McNutt, M.K., Zhu, Y.S., 1996. Mapping the descent of Indian and Eurasian plates beneath the Tibetan Plateau from gravity anomalies. Journal of Geophysical Research 101 (B5), 11275–11290.

John, B., Zhou, X., Li, J., 1990. Formation and tectonic evolution of southeastern China and Taiwan: isotopic and geochemical constraints. Tectonophysics 183 (1), 145–160.

Jordan, T., Watts, A., 2005. Gravity anomalies, flexure and the elastic thickness structure of the India–Eurasia collisional system. Earth and Planetary Science Letters 236 (3–4), 732–750.

Kenneth, J.H., Chen, H.H., 1999. Geologic Atlas of China. Elsevier, Amsterdam, p. 362.

Kim, S.W., Kwon, S., Koh, H.J., Yi, K., Jeong, Y.J., Santosh, M., 2011. Geotectonic framework of Permo–Triassic magmatism within the Korean Peninsula. Gondwana Research 20, 865–889.

Kirby, J.F., Swain, C.J., 2009. A reassessment of spectral Te estimation in continental interiors: the case of North America. Journal of Geophysical Research 114, B08401.

Kirby, J., Swain, C., 2011. Improving the spatial resolution of effective elastic thickness estimation with the fan wavelet transform. Computers & Geosciences 37 (9), 1345–1354.

Li, S., Santosh, M., Zhao, G., Zhang, G., Jin, C., 2012a. Intracontinental deformation in a frontier of super-convergence: a perspective on the tectonic milieu of the South China Block. Journal of Asian Earth Sciences 49 (0), 313–329.

Li, X., 1994a. A comprehensive U–Pb, Sm–Nd, Rb–Sr and 40/Ar–39/Ar geochronological study on Guidong Granodiorite, southeast China: records of multiple tectonothermal events in a single pluton. Chemical Geology 115 (3), 283–295.

Li, Z., 1994b. Collision between the North and South China blocks: a crustal-detachment model for suturing in the region east of the Tanlu fault. Geology 22 (8), 739–742.

Li, Z.X., Li, X.H., 2007. Formation of the 1300-km-wide intracontinental orogen and postorogenic magmatic province in Mesozoic South China: a flat–slab subduction model. Geology 35 (2), 179–182.

Li, Z.X., Zhang, L., Powell, C.M.A., 1995. South China in Rodinia: part of the missing link between Australia–East Antarctica and Laurentia? Geology 23 (5), 407.

Li, Z.X., Li, X., Zhou, H., Kinny, P.D., 2002. Grenvillian continental collision in south China: new SHRIMP U–Pb zircon results and implications for the configuration of Rodinia. Geology 30 (2), 163–166.

Li, Z.X., Li, X.H., Chung, S.L., Lo, C.H., Xu, X., Li, W.X., 2012b. Magmatic switch-on and switch-off along the South China continental margin since the Permian: transition from an Andean-type to a Western Pacific-type plate boundary. Tectonophysics 532–535 (0), 271–290.

Lowry, A.R., Smith, R.B., 1995. Strength and rheology of the western US Cordillera. Journal of Geophysical Research 100 (B9), 17947–17963.

Maggi, A., Jackson, J., McKenzie, D., Priestley, K., 2000. Earthquake focal depths, effective elastic thickness, and the strength of the continental lithosphere. Geology 28 (6), 495–498.

Mao, X., Wang, Q., Liu, S., Xu, M., Wang, L., 2012. Effective elastic thickness and mechanical anisotropy of South China and surrounding regions. Tectonophysics 550–553, 47–56.

Mareschal, J., Jaupart, C., 2004. Variations of surface heat flow and lithospheric thermal structure beneath the North American craton. Earth and Planetary Science Letters 223 (1), 65–77.

McKenzie, D., Nimmo, F., 1997. Elastic thickness estimates for Venus from line of sight accelerations. Icarus 130 (1), 198–216.

Northrup, C., Royden, L., Burchfiel, B., 1995. Motion of the Pacific plate relative to Eurasia and its potential relation to Cenozoic extension along the eastern margin of Eurasia. Geology 23 (8), 719–722.

Pérez-Gussinyé, M., Watts, A., 2005. The long-term strength of Europe and its implications for plate-forming processes. Nature 436 (7049), 381–384.

Pérez-Gussinyé, M., Lowry, A., Watts, A., 2007. Effective elastic thickness of South America and its implications for intracontinental deformation. Geochemistry, Geophysics, Geosystems 8 (5), 22.

Pérez-Gussinyé, M., Lowry, A.R., Watts, A.B., Velicogna, I., 2004. On the recovery of effective elastic thickness using spectral methods: examples from synthetic data and from the Fennoscandian Shield. Journal of Geophysical Research 109, B10409. http://dx.doi.org/10.1029/2003JB002788.

Pérez-Gussinyé, M., Lowry, A., Morgan, J.P., Tassara, A., 2008. Effective elastic thickness variations along the Andean margin and their relationship to subduction geometry. Geochemistry, Geophysics, Geosystems 9 (2), Q02003. http://dx.doi.org/10.1029/2007GC001786.

Pérez-Gussinyé, M., Swain, C., Kirby, J., Lowry, A., 2009a. Spatial variations of the effective elastic thickness, Te, using multitaper spectral estimation and wavelet methods: examples from synthetic data and application to South America. Geochemistry, Geophysics, Geosystems 8, Q05009.

Pérez-Gussinyé, M., Metois, M., Fernández, M., Vergés, J., Fullea, J., Lowry, A., 2009b. Effective elastic thickness of Africa and its relationship to other proxies for lithospheric structure and surface tectonics. Earth and Planetary Science Letters 287 (1–2), 152–167.

Panza, G., Raykova, R., 2008. Structure and rheology of lithosphere in Italy and surrounding. Terra Nova 20 (3), 194–199.

Panza, G.F., Pontevivo, A., Chimera, G., Raykova, R., Aoudia, A., 2003. The lithosphere–asthenosphere: Italy and surroundings. Episodes-Newsmagazine of the International Union of Geological Sciences 26 (3), 169–174.

Pavlis, N.K., Holmes, S.A., Kenyon, S.C., Factor, J.K., 13–18 April 2008. An Earth Gravitational Model to Degree 2160: EGM2008. EGU General Assembly.

Richter, C.F., 1958. Elementary Seismology.

Shen, W.Z., Zhu, J.C., Liu, C.S., Ling, H.F., 1993. Sm–Nd isotopic study of basement metamorphic rocks in South China and its constraint on material sources of granitoids. Acta Petrologica Sinica 9 (2), 115–124.

Tao, W., Shen, Z., 2008. Heat flow distribution in Chinese continent and its adjacent areas. Progress in Natural Science 18 (7), 843–850.

Wang, Q.C., 2009. Preliminary discuss ion on sedimentary tectonics of the clustered continents of South China. Acta Sedimentologica Sinica 27 (5), 811–817 (in Chinese with English abstract).

Wang, Y., 2001. Heat flow pattern and lateral variations of lithosphere strength in China mainland: constraints on active deformation. Physics of the Earth and Planetary Interiors 126 (3–4), 121–146.

Wang, Y.J., Fan, W.M., Guo, F., Peng, T., Li, C., 2003. Geochemistry of Mesozoic mafic rocks adjacent to the Chenzhou-Linwu fault, South China: implications for the lithospheric boundary between the Yangtze and Cathaysia blocks. International Geology Review 45 (3), 263–286.

Wang, D., Shu, L., 2012. Late Mesozoic basin and range tectonics and related magmatism in Southeast China. Geoscience Frontiers 3 (2), 109–124.

Wang, Y., Fan, W., Zhang, G., Zhang, Y., 2013. Phanerozoic tectonics of the South China Block: key observations and controversies. Gondwana Research 23, 1273–1305.

Watts, A., Burov, E., 2003. Lithospheric strength and its relationship to the elastic and seismogenic layer thickness. Earth and Planetary Science Letters 213 (1–2), 113–131.

Watts, A.B., 2001. Isostasy and Flexure of the Lithosphere. Cambridge University Press.

Wu, J., Zhang, Z., 2012. Spatial distribution of seismic layer, crustal thickness, and Vp/Vs ratio in the Permian Emeishan Mantle Plume region. Gondwana Research 22 (1), 127–139.

Zhang, Z.J., Wang, Y.H., Chen, Y., Houseman, G.A., Tian, X.B., Wang, E.Q., Teng, J.W., 2009. Crustal structure across Longmenshan fault belt from passive source seismic profiling. Geophysical Research Letters 36, L17310.

Zhang, Z., Yang, L., Teng, J., Badal, J., 2011. An overview of the earth crust under China. Earth-Science Reviews 104 (1–3), 143–166.

Zhang, Z., Wu, J., Deng, Y., Teng, J., Zhang, X., Chen, Y., Panza, G., 2012. Lateral variation of the strength of lithosphere across the eastern North China Craton: new constraints on lithospheric disruption. Gondwana Research 22 (3–4). http://dx.doi.org/10.1016/j.gr.2012.03.006.

Zhang, Z., Deng, Y., Chen, L., Wu, J., Teng, J., Panza, G., 2013. Seismic structure and rheology of the crust under mainland China. Gondwana Research 23 (4), 1455–1483.

Zhou, X., Li, W., 2000. Origin of Late Mesozoic igneous rocks in Southeastern China: implications for lithosphere subduction and underplating of mafic magmas. Tectonophysics 326 (3–4), 269–287.

Zhou, X., Zhu, Y., 1993. Late Proterozoic collisional orogen and geosuture in southeastern China: petrological evidence. Chinese Journal of Geochemistry 12, 239–251 (in Chinese with English abstract).